Characterization of multicomponent counter-diffusion in silicalite : Application to C6 isomers in liquid phase

TAYAKOUT Mélaz, JOLIMAITRE Elsa, DUBREUIL Anne-Claire et METHIVIER Alain

Institut Français du Pétrole (IFP), BP 3, 69390 Vernaison

Introduction

In literature, diffusion of mixtures in microporous solids is usually studied in the low concentration regime, where the solid porosity is not fully occupied by adsorbed molecules. It corresponds to experimental conditions which are unfavourable to adsorption, typically measurements in the phase gas at low partial pressures and/or high temperatures (1). In such conditions, exploitation of the experimental data can be carried out by models such as those developed by Krishna (theory of Maxwell-Stefan applied to the diffusion in the solids via the model known as of the "Dusty Gas Model").

When separation by adsorption is carried out in the liquid phase, which is industrially very frequent, the confinement of the molecules in the porous network is very high. Consequently, volume constraints are added to the kinetic and thermodynamic constraints (adsorption equilibrium) of the system: a given specie can penetrate in the solid only if the corresponding volume is available within the network. This type of constraint is not taken into account in the traditional kinetic models. In order to introduce this constraint, a new mass transfer model based on the "Dusty Gas Model" is proposed. This model is coupled with a thermodynamic model which describes the adsorption of the different components with a generalized monosite Langmuir isotherm.

The model is validated by comparison with experimental liquid phase breakthrough curves for ternary mixtures of various hexane isomers in silicalite. The model represents the co-diffusion and the counter-diffusion of these molecules with a high degree of accuracy, even though the diffusion kinetics of these molecules are very different in silicalite. Moreover, the Maxwell-Stefan diffusion coefficients used for the simulations are completely coherent with values obtained for pure components at low concentration.

Model

Our experimental set-up is a column packed with bi-disperse pellets composed of zeolite crystals held together by a binder. Such a system is classically divided into three phases: the bulk fluid, the particles filled with macropores and the crystals containing the microporosity where adsorption occurs (2). The pellets and the microporous particles are supposed to be spherical. A mass balance can be written for an adsorbate i in each of these phases.

The packed bed is represented by forty CSTR (continuous stirred tank reactor). The breakthrough curve being stiff , this approach by CSTR seems the better way to numerically solve this stiff problem. Mass transfer resistance at the

particle surface and in the macropores are lumped into a single external film mass transfert coefficient k^m. For numerical reasons, a stagnant film around the zeolite crystals is also introduced, but the corresponding mass transfer coefficient k^c is always set so as to make this resistance negligible. The microporous solid chosen for this study is silicalite (a MFI type zeolite), whose pore diameter (around 5-5.5 $\overset{\circ}{A}$) is very close to alkanes molecule size. Therefore, diffusion in the crystals is supposed to occur only by microporous diffusion .

Mass transfer in the zeolite is described by the Stephan – Maxwell (3) equations adapted to diffusion in a porous solid (Dusty Gas Model). The transport model proposed in this paper is comparable to the very well known model published by Krishna in 1990 (4). However several modifications were introduced to this model:

1. In the different publications (4, 5, 6) a flow corresponding to the vacant sites is introduced and the sum of components flows plus the flow corresponding to the vacant sites is supposed to be zero.   Moreover, the authors end up by cancelling the flow corresponding to the vacant sites in order to preserve binary counterdiffusion between two components (1 and 2). This supposes an implicit dependence between the diffusion coefficients of the various species.
In order to suppress this dependence, the flow corresponding to the vacant sites is not cancelled in our model .

2. The surface chemical potential gradients in the Dusty Gaz Model may be expressed as a function of the molar fraction gradient by introducing the thermodynamic factors matrix. In the elements of this matrix appears a term $\dfrac{1}{1-\theta_t}$.

At the saturation of the solid, θ_t is equal to one and the term in $\dfrac{1}{1-\theta_t}$ becomes undetermined. In this paper, a variable change (7, 8) is proposed in order to raise this indetermination. The new state variable is the hypothetical bulk phase concentration in equilibrium with the adsorbed phase. To introduce constraints corresponding to geometrical volume conservation, the chosen state variable is the volume fraction.

At saturation, if the molecules molar volumes are equivalents, the velocity variation is negligible.

With all the hypothesis presented above, the model's equations are:
In the bulk fluid:
The first CSTR

$$
\begin{bmatrix} \dfrac{L}{v_0^f}\dfrac{\partial \phi_1^{f,1}}{\partial t} \\ . \\ . \\ . \\ \dfrac{L}{v_0^f}\dfrac{\partial \phi_{nc-1}^{f,1}}{\partial t} \end{bmatrix} = \begin{bmatrix} \left(\phi_1^e - \phi_1^{f,1}\right) + \dfrac{L}{v_0^f}\dfrac{3(1-\varepsilon_i)\varepsilon_p}{\varepsilon_i R_p}k_1^m\left(\phi_1^{m,1} - \phi_1^{f,1}\right) \\ . \\ . \\ . \\ \left(\phi_{nc-1}^e - \phi_{nc-1}^{f,1}\right) + \dfrac{L}{v_0^f}\dfrac{3(1-\varepsilon_i)\varepsilon_p}{\varepsilon_i R_p}k_{nc-1}^m\left(\phi_{nc-1}^{m,1} - \phi_{nc-1}^{f,1}\right) \end{bmatrix} \qquad \mathbf{1}
$$

The ith CSTR

$$\begin{bmatrix} \dfrac{L}{v_0^f}\dfrac{\partial \phi_1^{f,i}}{\partial t} \\ . \\ . \\ . \\ \dfrac{L}{v_0^f}\dfrac{\partial \phi_{nc-1}^{f,i}}{\partial t} \end{bmatrix} = \begin{bmatrix} \left(\phi_1^{f,i-1}-\phi_1^{f,i}\right)+\dfrac{L}{v_0^f}\dfrac{3(1-\varepsilon_i)\varepsilon_p}{\varepsilon_i R_p}k_1^m\left(\phi_1^{m,i}-\phi_1^{f,i}\right) \\ . \\ . \\ . \\ \left(\phi_{nc-1}^{f,i-1}-\phi_{nc-1}^{f,i}\right)+\dfrac{L}{v_0^f}\dfrac{3(1-\varepsilon_i)\varepsilon_p}{\varepsilon_i R_p}k_{nc-1}^m\left(\phi_{nc-1}^{m,i}-\phi_{nc-1}^{f,i}\right) \end{bmatrix}$$

2

The constraints associated to these equations are:

$$\sum_{j=1}^{nc}\phi_j^{f,i}=1 \qquad \text{i=1, ... , N}_{\text{CSTR}}$$

3

In the ith CSTR, the equations associated to the macroporosity can be written :

$$\begin{bmatrix} \dfrac{\partial \phi_1^{m,i}}{\partial t} \\ . \\ . \\ \dfrac{\partial \phi_{nc-1}^{m,i}}{\partial t} \end{bmatrix} = \begin{bmatrix} -\dfrac{3}{R_p}k_1^m\left(\phi_1^{m,i}-\phi_1^{f,i}\right)-\dfrac{3(1-\varepsilon_p)}{\varepsilon_p R_c}k_1^c\left(\phi_1^{m,i}-\phi_1^{*,i}\right) \\ . \\ . \\ -\dfrac{3}{R_p}k_1^m\left(\phi_{nc-1}^{m,i}-\phi_{nc-1}^{f,i}\right)-\dfrac{3(1-\varepsilon_p)}{\varepsilon_p R_c}k_{nc-1}^c\left(\phi_{nc-1}^{m,i}-\phi_{nc-1}^{*,i}\right) \end{bmatrix}$$

4

The constraints associated to these equations are:

$$\sum_{j=1}^{nc}\phi_j^{m,i}=1 \qquad \text{i=1, ... , N}_{\text{CSTR}}$$

5

In the ith CSTR, the equations associated to the mass balance of the the jth component plus this one associated to vacant sites in the crystal can be written as:

$$\dfrac{\partial \phi_j^{c,i}}{v^0 \partial t}=-\dfrac{1}{r^2}\dfrac{\partial\left(r^2 N_j^{c,i}\right)}{\partial r} \qquad \text{j=1, ..., nc +1}$$

6

The constraints associated to these equations are:

$$\sum_{j=1}^{nc+1}\phi_j^{c,i}=1 \qquad \text{i=1, ... , N}_{\text{CSTR}}$$

7

$$\sum_{j=1}^{nc+1}N_j^{c,i}=0 \qquad \text{i=1, ... , N}_{\text{CSTR}}$$

8

The state variable chosen is the hypothetical bulk phase variable in equilibrium with the adsorbed phase called $\phi_j^{*,i}$. The relation between the two variable $\phi_j^{*,i}$ and $\phi_j^{c,i}$ is given by the generalised Langmuir law as follows:

$$\phi_j^{c,i} = \frac{q^{max} b_j \phi_j^{*,i}}{1 + \sum_{k=1}^{nc} \frac{b_k \phi_k^{*,i}}{v^0}}$$

9

Introducing this variable $\phi_j^{*,i}$ and the constraint corresponding to equation 7 in equation 6 gives for all components:

$$\begin{bmatrix} b_1 q^{max}\left(1 + \sum_{\substack{j=1 \\ j\neq 1}}^{nc} b_i \frac{\phi_i^{*,i}}{v}\right) & \cdots & -b_1 b_{nc} q^{max} \frac{\phi_1^{*}}{v} \\ \cdot & & \cdot \\ \cdot & & \cdot \\ \cdot & & \\ -b_1 b_{nc} q^{max} \frac{\phi_{nc}^{*}}{v} & \cdots & +b_{nc} q^{max}\left(1 + \sum_{\substack{j=1 \\ j\neq nc}}^{nc} b_i \frac{\phi_i^{*,i}}{v}\right) \end{bmatrix} \begin{bmatrix} \dfrac{\partial \phi_1^{*,i}}{\partial t} \\ \cdot \\ \cdot \\ \dfrac{\partial \phi_{nc}^{*,i}}{\partial t} \end{bmatrix} = \begin{bmatrix} -\dfrac{1}{r^2}\dfrac{\partial\left(r^2 N_1^{c,i}\right)}{\partial r} \\ \cdot \\ \cdot \\ -\dfrac{1}{r^2}\dfrac{\partial\left(r^2 N_{nc}^{c,i}\right)}{\partial r} \end{bmatrix}$$

10

The boundary conditions in the ith CSTR for the jth component are :

$\forall t$ At $r = 0$ $N_j^{c,i} = 0$

         At $r = R_c$ $N_j^{c,i} = k_j^c (\phi_j^{m,i} - \phi_j^{*,i})$

The flux $N_j^{c,i}$ is given by the Dusty Gaz Model (9). Constraints corresponding to equations 7 and 8 and the new state variable corresponding to the bulk phase are introduced in the Dusty Gas Model. The state variable corresponding to bulk phase is introduced via the generalised Langmuir law (equation 9). The DGM becomes the following system of equations:

$$\begin{bmatrix} q^{max} b_1 \dfrac{\partial \phi_1^{*,i}}{\partial r} \\ \cdot \\ \cdot \\ q^{max} b_{nc} \dfrac{\partial \phi_{nc}^{*,i}}{\partial r} \end{bmatrix} = \begin{bmatrix} \dfrac{1}{D_{1,nc+1}}\left(\dfrac{1 + \sum_{i=1}^{nc} b_i \frac{\phi_i^{*,i}}{v}}{q^{max}} - \sum_{\substack{k=1 \\ k\neq i}}^{nb} b_k \phi_k^{*,i}\right) & \cdots & \left(\dfrac{b_1 \phi_1^{*,i}}{D_{1,nc+1}}\right) \\ \cdot & & \cdot \\ \cdot & & \cdot \\ \left(\dfrac{b_{nc}\phi_{nc}^{*,i}}{D_{nc,nc+1}}\right) & \cdots & \dfrac{1}{D_{nc,nc+1}}\left(\dfrac{1 + \sum_{i=1}^{nc} b_i \frac{\phi_i^{*,i}}{v}}{q^{max}} - \sum_{\substack{k=1 \\ k\neq i}}^{nc} b_k \phi_k^{*,i}\right) \end{bmatrix} \begin{bmatrix} N_1^{c,i} \\ \cdot \\ \cdot \\ N_{nc}^{c,i} \end{bmatrix}$$

11

The flux vector is obtained by inversion of this matrix and can be calculated from the volume fraction gradient. The flux are then introduced in equations 10. These equations are integrated after inversion of the matrix.

Numerical Solution of Model Equations

The set of partial differential equations are reduced first to a set of ordinary differential equations applying an orthogonal collocation technique to the spatial coordinate corresponding to the crystal. Subroutines JCOBI and DFOPR developed by Villadsen and Michelsen (10) were used. The spatial coordinate corresponding

to the bed length are solved by a CSTR approach (using forty CSTR). The resulting ordinary differential-algebraic system of equations is solved by the DDASPG integration subroutine (IMSL library), based on the Petzold-Gear BDF method. The two matrix are inversed by the DLINRG inversion subroutine (IMSL library).

Materials and Methods

Adsorbent Characterization

The silicalite crystals used in this study were supplied by Zeolist International. The Si/Al ratio, measured by X-ray fluorescence, is 500 ± 50%. The few H^+ cations were replaced by Na^+ cations using the conventional ion exchange technique and subsequent washing. Scanning electron microscopy showed that they consisted of spherical crystals with mean crystal radius of R_C=0.75 10^{-6} m.

This zeolite was pelletized with a silica binder in the Institut Français du Pétrole then cut and sieved. Extrudates are small cylinders with a diameter of 0.7 mm and a mean length of 0.8 mm. For model simplification, particles were supposed to be spherical with a mean radius of R_P=5 10^{-4} m. The binder ratio, determined from n-hexane adsorption gravimetric uptake experiments performed with both crystals and particles, is 20 %.

Prior to experiments, the sample has been activated in a nitrogen stream for 3 h at 300°C.

Experimental setup

Breakthrough experiments which allow to evaluate both thermodynamic and mass transfer data were performed (2) . The dynamic adsorption unit is described in figure 1. A stainless steel column (L=1 m and S=4.415 10^{-5} m²) is filled with a known amount of particles and placed into the oven. First the column is filled with the solvent (or desorbent) which is also an adsorbable species. Then the feed is injected in the column until complete breakthrough (outlet concentration = inlet concentration). During the experiment the whole column is maintained at 35 bar and 185°C. Liquid fractions of the effluent are collected and analyzed by a gas chromatograph with FID detector and PONA analytical column. The concentrations at the outlet of the column are plotted as fractional volumes as a function of time ; they are called "breakthrough curves". Reverse breakthrough experiment consists in injecting the solvent in a column filled with the feed.
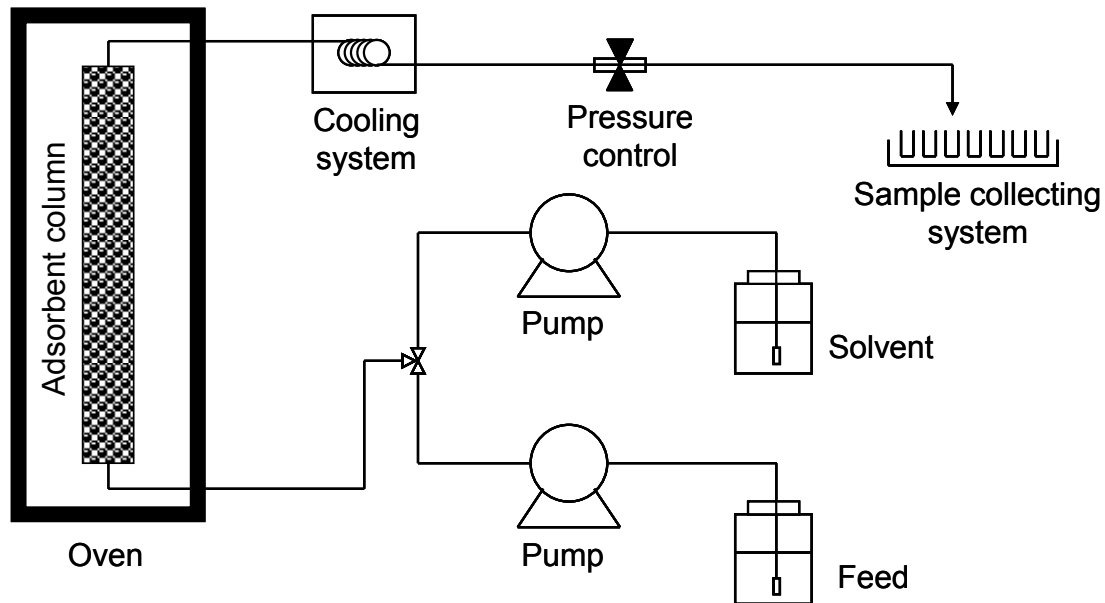
Figure 1: Schematic view of the testing device

2-methylpentane (2MP) and 3-methylpentane (3MP) were purchased from Fluka Chemika. 2,3-dimethylbutane (23DMB) and 2,2-dimethylbutane (22DMB) were purchased from SAFC. The specified purities are over 99 %. Tri-isopropyl-benzene (TiPB) was purchased from Acros Organics with a specified purity over 97 %. All these adsorbates were used without further specification.

Results and Discussion

Ternary breakthrough curves

Complete information on the experimental fixed bed runs is detailed in Tables 1 and 2. Informations concerning geometrical parameters are given in Table 1 and the experimental conditions are given in Table 2.

Run 1,2 and 5 were used to estimate the model parameters (both kinetic and thermodynamic parameters). Model validation was performed with the other runs (3, 4, 6, and 7) without any parameter estimation. The estimated model parameters are specified in Table 3.

Table 1. Geometrical parameters

ε_i (-)	0.355
ε_p (-)	0.33
S (m²)	4.415 10^{-5}
L_{bed} (m)	1
R_C (m)	0.75 10^{-6}
R_P (m)	5 10^{-4}

Table 2. Experimental conditions

Constant experimental conditions

Temperature (K)   458

Pressure (Pa)   3.5 10^6

mass of adsorbent (g)   37.13

		Experimental conditions				
run	comp.	volume fraction in the feed ϕ_i^e (-)	initial volume fraction ϕ_i^i (-)	velocity v_0^f (m/s)	Figure	Estimated Parameter
1	2MP	0.0008	0.9991	5.8 10^{-3}	(fig. 2)	$D_{2MP,nc+1}$
	TiPB	0.079	0.0			k^m
	3MP	0.9202	0.0009			$D_{3MP,nc+1}$
2	2MP	0.0066	0.9958	4.8 10^{-3}	(fig. 3a)	
	23DMB	0.494	0.0033			$D_{23MB,nc+1}$
	3MP	0.4994	0.0009			
3	2MP	0.0071	0.9958	4.8 10^{-3}	(fig. 3d)	
	23DMB	0.2897	0.0033			
	3MP	0.7032	0.0009			
4	2MP	0.9948	0.0027	5.8 10^{-3}	(fig. 3c)	
	23DMB	0.0038	0.2979			
	3MP	0.0014	0.6994			
5	2MP	0.9959	0.0042	5.8 10^{-3}	(fig. 3b)	b_{2MP}
	23DMB	0.0032	0.6344			b_{23DMB}
	3MP	0.0009	0.3614			$b_{3MP,}$
6	2MP	0.004	0.999	5.8 10^{-3}	(fig. 4b)	
	22DMB	0.5188	0.0039			
	3MP	0.4772	0.0071			
7	2MP	0.0022	0.999	5.8 10^{-3}	(fig. 4a)	
	22DMB	0.8095	0.0			$D_{22MB,nc+1}$
	3MP	0.1883	0.001			

Table3. Model Parameters

Kinetic parameters

Component	molar volume v (m³/mol)	Maxwell-Stefan diffusion coefficient $D_{i,nc+1}$ (m²/s)	mass transfer coefficient around the particles k_i^m (m/s)	mass transfer coefficient around the crystals k_i^c (m/s)
2MP	$1.93 10^{-4}$	$6\ 10^{-15}$	8.10^{-4}	9.10^{-3}
TiPB	$1.7 10^{-4}$	-	8.10^{-4}	9.10^{-20}
3MP	$1.86 10^{-4}$	$4\ 10^{-14}$	8.10^{-4}	9.10^{-3}
23DMB	$1.87 10^{-4}$	$1\ 10^{-16}$	8.10^{-4}	9.10^{-3}
22DMB	$1.99 10^{-4}$	$6\ 10^{-17}$	8.10^{-4}	9.10^{-3}

Thermodynamic parameters

component	saturation concentration q^{max} (mol/m³)	thermodynamic coefficient b_i (m³/mol)
2MP	1000	1
TiPB	-	-
3MP	1000	0.5
23DMB	1000	1
22DMB	1000	1

Ternary breakthrough curve 3MP-TiPB-2MP

Figure 2 shows the comparison between experimental and simulated breakthrough curves obtained for run 1 with a feed composed of a mixture of 3MP (90%) and TiPB (10%). The solvent initially present in the column is 2MP. The kinetic parameters for the 3 components are estimated from these experimental data. The simulated breakthrough curves on Figure 2 are obtained with the optimised parameters. The agreement between experience and simulation is very satisfactory. TiPB's molecular diameter ($8.6\ \overset{\circ}{A}$) doesn't allow this molecule to enter in the silicalite porosity (11). The mass transfer coefficient corresponding to the crystal resistance k^c is therefore fixed at a negligible value of 9.10^{-20} m s^{-1}. Moreover, the TiPB breakthrough curve allows us to estimate the mass transfer resistance in the macropores and the number of CSTR. The conclusion, valid for all the experiments presented in this paper, is that resistance is essentially due to mass transfer in the zeolite micropores (macropore resistance is negligible).

The thermodynamic Langmuir parameters could not be estimated from these experimental data because they are not sensitive enough.
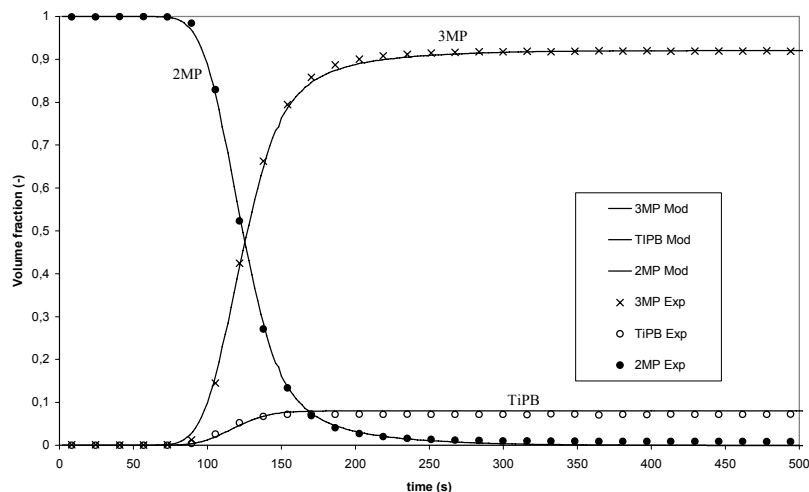
Figure 2: Ternary breakthrough curves for mixtures of 3MP (90%) - TiPB (10%) in 2MP (100%). run 1 . The experimental conditions and model parameters are specified in Tables 1, 2 and 3. The lines represent model predictions, and the points are experimental data.

Ternary breakthrough curves 3MP-23MB-2MP

Figures 3 a) and d) show the breakthrough curves of mixtures of 3MP and 23DMB at different compositions in solvent 2MP (runs 2 and 3). Figures 3 b) and c) show the corresponding desorption breakthrough curves (runs 5 and 4). The only model parameters that are estimated from these experimental data are:
- the 23DMB Maxwell-Stefan diffusion coefficient from run 2 (fig. 3a),
- the thermodynamical parameters of these 3 molecules (the saturation concentration being fixed) from run 5 (fig. 3b).

The concentrations in the adsorbed phase at saturation qmax have been measured independently and do not need to be estimated from these experiments.

Figure 3 c) and d) show the validation of the model with the previously estimated parameters. It can be seen that the model represents very well the experimental curves.
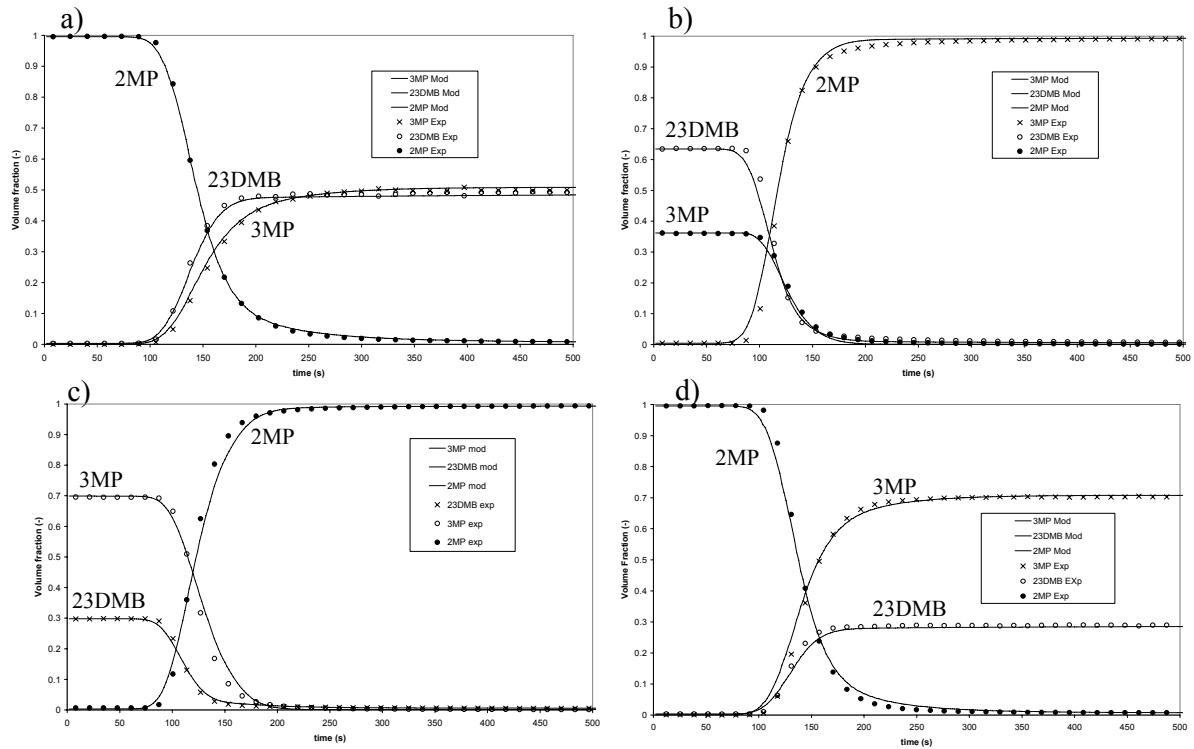
Figure 3: Ternary breakthrough curves for mixtures of 3MP – 23DMB - 2MP. The experimental conditions and model parameters are specified in tables 1, 2 (run 2 for a), run 3 for d), run 4 for c) and run 5 for b)) and 3. The lines represent model predictions, and the points are experimental data.

Ternary breakthrough curves 3MP-22DMB-2MP

The same method was used to estimate the 22DMB kinetic parameters from run 7. The 22DMB thermodynamic parameter b is not sensitive enough and could only be estimated from the desorption curve not shown in this paper.

Figures 4 a) and b) show the breakthrough mixtures of 3MP and 22DMB curves obtained for runs 6 and 7 at different compositions and 2MP as solvent. Figure 4 b) shows the validation of the model and of the estimated parameter. Once again, the simulated curves represent very well the experimental data, showing the ability of the model to predict the system behaviour.
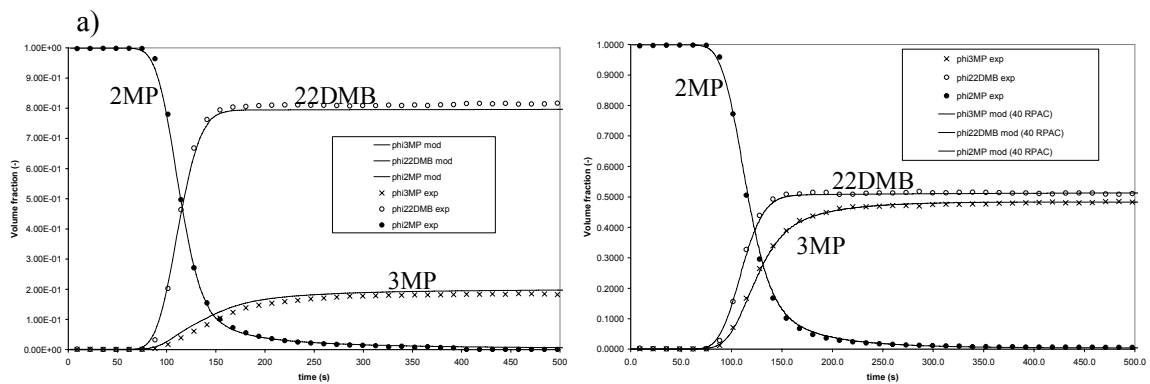
Figure 4: Ternary breakthrough curves for mixtures of 3MP – 22DMB - 2MP. The experimental conditions and model parameters are specified in tables 1, 2 (run 7 for a), run 6 for b)) and 3. The lines represent model predictions, and the points are experimental data.

Discussion

The new model proposed in this paper is a very useful tool for estimating kinetic and thermodynamic adsorption parameters from liquid phase breakthrough curves.

Moreover, estimated Maxwell-Stefan diffusion coefficients for the different alkane molecules are consistent with literature values (12). This is all the more surprising since literature Maxwell-Stefan diffusion coefficients were obtained in very different experimental conditions, that is to say gas phase experiments at very low silicalite loading.

Liquid phase breakthrough curves are however not very well adapted for thermodynamic parameters (Langmuir coefficients b) estimation. In liquid phase experiments, the microporosity is permanently filled with molecules. When the liquid feed composition is varied, an exchange between the feed and the solvent molecules takes place in the zeolite pores. The breakthrough curve is therefore not very sensitive to the pure components isotherms, and the Langmuir parameters shown on Table 3 have to be taken with caution.

Conclusion

In this paper, a new model is proposed, based on the Stephan – Maxwell equations adapted to diffusion in porous solids (Dusty Gas Model). Compared to former literature models, the main modifications are:
- the independence of all the species Maxwell-Stefan diffusion coefficients,
- the suppression of the effective diffusion coefficients indetermination at the adsorption saturation.

The model is first used for parameter estimation from experimental liquid breakthrough curves of 2MP, 3MP, 23DMB and 22DMB in packed bed filled with a silicalite zeolite. The Maxwell-Stefan diffusion coefficients are estimated with a good precision and are coherent with literature. The thermodynamic parameters are not very sensitive and therefore not estimated with a good precision. The model is then validated by simulation of independent experimental data. A good agreement is obtained between experimental data and the model. Multicomponent diffusion at adsorption saturation in MFI zeolite is thus correctly represented by the proposed model.

Nomenclature

b_i : thermodynamic coefficient of component i (m^3/mol)

c_t : total concentration (mol/m^3)

$D_{i,nc+1}$: Maxwell-Stefan diffusion coefficient of component i (m^2/s)

k_i^c : mass transfer coefficient of component i corresponding to the crystal (m/s)

k_i^m : mass transfer coefficient of component i corresponding to the macroporosity (m/s)

L : packed column length (m)

nc: number of components (-)

$N_i^{c,j}$: molar flux of component i in the jth CSTR $(\mathrm{mol/m^2 s})$

N_{CSTR} : Number of CSTR (continuous stirred tank reactors)

q^{max} : saturation concentration $(\mathrm{mol/m^3\, of\, solid})$

q_i : concentration of adsorbaded phase $(\mathrm{mol/m^3 of\, solid})$

R_c : crystal radius(m)

R_P: pellet radius (m)

S : section of the column (m²)

T : temperature (K)

v : molar volume of mixture $\left(v = \dfrac{1}{C} \right)$ $(\mathrm{m^3/mol})$

v_f^0: interstitial velocity (m/s)

ε_i : extra granular porosity (-)

ε_p : intra granular porosity (-)

$\phi_i^{c,j}$: volume fraction of component i adsorbed on solid in the jth CSTR (-)

ϕ_i^i : volume fraction of component i initially in the bed (at t = 0) (-)

ϕ_i^e : volume fraction of component i in the feed (-)

$\phi_i^{*,j}$: volume fraction of component i in the hypothetic fluid at equilibrium with the adsorbed phase in the jth CSTR (-)

$\phi_i^{m,j}$: volume fraction of component i in the macroporosity in the jth CSTR (-)

$\phi_i^{f,j}$: volume fraction of component i in the extragranular fluid phase in the jth CSTR (-)

θ_t : total molar fraction of adsorbed phase (-)

μ_i : chemical potential (J/mol)

References

1.   Barcia P.S., Silva J.A.C., and Rodrigues A.E. (2006), Separation by Fixed-Bed Adsorption of Hexane Isomers in Zeolite BETA Pellets, *Ind. Eng. Chem. Res.*, 45, 4316

2.   Ruthven, D.M. (1984), Principles of adsorption and adsorption processes, John Wiley & Sons ed.

3.   Taylor, R.; Krishna, R. , *Multicomponent Mass Transfer* (1993); John Wiley & Sons: New York

4.   R. Krishna, "Multicomponent surface diffusion of absorbed species: a description based on the generalized Maxwell-Stefan equations, Chemical Engineering Science, vol. 45, No 7, pp 1779-1791 (1990)

5.   R. Krishna, "A united approach to the modelling of intraparticule diffusion in adsorption processes"(1993), Gas Separation&Purification, vol 7, No 2, pp 91-104

6.   R. Krishna, J.M. van Baten (2005), "Diffusion of alkane mixtures in zeolites: Validating the Maxwell-Stefan Formulation using MD Simulations", J. Phys. Chem. B, 109, 6386

7.   Tayakout-Fayolle, M.; Jolimaitre, E.; Jallut, C. (2000), Consequence of structural identifiability properties on state-model formulation for linear inverse chromatography. *Chem. Eng. Sci.*, *55*, 2945.

8.   Couenne, F.; Jallut, C.; Tayakout-Fayolle, M. (2005), On minimal representation of heterogeneous mass transfer for simulation and parameter estimation: application to breakthrough curves exploitation. *Comp. and Chem. Engng.*, *30*, 42.

9.   Krishna R, Wesselingh JA, "The Maxwell-Stefan approach to mass transfer", Chemical Engineering Science, vol. 52, No 6, pp. 861-911 (1997)

10.   Villadsen, J.; Michelsen, M.L. (1978), *Solution of Differential Equation Models by Polynomial Approximation*. Prentice-Hall, Englewood Cliffs: NJ.

11.   Sano, T., Kawakami, M., Kiyozumi, Y., Yanagishita, H., Kitamoto, D., Mizukami, F. (1994), Potentials of silicalite membranes for the separation of alcohol/water mixtures, Zeolites and related microporous materials : State of the art, Studies in Surface Science and Catalysis, vol.84

12.   Jolimaitre, E.; Tayakout-Fayolle, M.; Jallut, C.; Ragil, K. (2001), Determination of mass transfer and thermodynamic properties of branched paraffins in silicalite by inverse chromatography technique. *Ind. Eng. Chem. Res.*, *40*, 914.